THE BALTIC JOURNAL
OF ROAD
AND BRIDGE
ENGINEERING
2024/19(2)

ISSN 1822-427X/eISSN 1822-4288
2024 Volume 19 Issue 2: 102–130
https://doi.org/10.7250/bjrbe.2024-19.638

STRESS AND STRAIN OF RCC PAVEMENT WITH CEMENT STABILIZED BASE DEPENDING ON LOAD AND SEASON OF THE YEAR

RAFAL MICKEVIČ*, AUDRIUS VAITKUS

Road Research Institute, Vilnius Gediminas Technical University, Vilnius, Lithuania

Received 8 January 2024; accepted 27 March 2024

Abstract. Slip-form concrete (JPCP) has a number of years of good performance experience. An alternative to slip-form concrete is roller-compacted concrete (RCC). The RCC mixture has a significantly larger number of fine aggregates, which leads the concrete mix to be non-slip and compacted by rollers. RCC has the strength and performance of conventional concrete or even higher. Due to all the advantages, the use of RCC pavement in industrial areas and low-volume rural roads is very beneficial. Experimental test section of RCC pavement structure with cement and special additives stabilized base (CTB) was installed on local road No. 130 in Lithuania, which was reconstructed in 2021. The main objective of this study is to learn about the environmental impact on the pavement structure. To reach our aim at the stage of reconstruction of the local road temperature, humidity sensors and a strain gauge were installed under the RCC layer and CTB. During the lifetime of pavement structure temperature and humidity data were collected daily and bearing capacity was measured during spring thaw. In addition, an artificial wheel load simulation using a falling weight deflectometer was performed at the location of the installed strain gauge to analyse deflections and to calculate stresses under RCC layer. The stresses under the RCC layer calculated from the strain gauge were also compared with the theoretical stress calculated at the design stage of the pavement structure

* Corresponding author. E-mail: rafal.mickevic@vilniustech.lt

Rafal MICKEVIČ (ORCID ID 0000-0003-0832-3536)
Audrius VAITKUS (ORCID ID 0000-0001-5103-9747)

to learn more about performance of the pavement structure. The results showed that slight changes in humidity at the bottom of the CTB had no significant influence on the deformations at the bottom of the RCC layer. Comparison of stresses under RCC layer showed that stresses calculated from strain gauge were 1.80 times lower than those calculated theoretically.

Keywords: bearing capacity, deflection, roller-compacted concrete, RCC, strain gauge, temperature-humidity sensor.

Introduction

Roller-compacted concrete (RCC) is a special mix of dry concrete that can be laid down with asphalt type paver and can be compacted with rollers. The RCC mixture can achieve high strengths levels due to compaction and aggregate interlock (Chhorn et. al., 2017). The consistency of the RCC mixture is very similar to conventional concrete mixture, but in different mixture proportion. RCC mixtures typically have a lower volume of cementitious materials, coarse aggregates (4–19 mm), and water than conventional concrete mixes and a higher volume of fine aggregates (0–4 mm), which fill the air voids in the pavement system (National Concrete Pavement Technology Center, 2010).

Pavement thickness is a crucial aspect in the pavement design; however, often a compromise between pavement performance and construction cost must be reached (Vaitkus et al., 2021). RCC could be laid down with a typical asphalt paver equipped with high-density screed and compacted with rollers. Due to the simplicity of the installation of the RCC layer, RCC could be laid down in a quicker way than conventional concrete (Sengun et. al., 2018). The use of the RCC instead of the slip-form concrete can reduce installation cost between 15% and 30% (Fardin & Goulart dos Santos, 2021; Mohammed & Adamu, 2018a; Ramezanianpour et. al., 2017; Modarres & Hosseini, 2014).

Fatigue is a phenomenon where weakening occurs in the material due to repeated load cycles. Pavement structures are constantly subjected to cyclic loads caused by vehicular traffic (Huang Yang, 2004). In concrete pavement structures, the concrete layer absorbs most of the stress resulting from loads. There are two types of stresses in the concrete layer – compressive and bending (Papagiannakis & Masad, 2008). When designing concrete pavement structures, the bending stresses occurring at the bottom of the concrete layer are the most critical, since the bending strength of concrete is lower than the compressive strength. When designing and calculating concrete pavement structures, it is very important to properly assess the resulting stresses and deformations at the bottom of the concrete layer. Repetitive bending stresses at the

bottom of the concrete layer affect the gradual loss of the load-bearing properties of the concrete (Lee & Barr, 2004). Calculations of concrete pavement constructions are based on fatigue functions, which are used to check the boundary conditions of the pavement construction. Depending on the applied calculation methods, different fatigue functions are used.

Depending on the design methodology, different mechanical properties of concrete are used. Designing concrete pavement structures according to *Richtlinien für die rechnerische Dimensionierung von Betondecken im Oberbau von Verkehrsflächen RDO Beton 09*, the two main properties – tensile elasticity modulus and tensile splitting strength – are used (Vaitkus et al., 2021). In design applications such as StreetPave or FAARFIELD, the most important mechanical property of concrete is flexural strength. Calculations with StreetPave are based on Mechanistic–Empirical Pavement Design Method. The design methodology used in StreetPave was taken from the PCA's Thickness Design for Concrete Highways and Streets manual. The procedure incorporates mechanistic components (load/stress/deflection) with empirical observations, including results from the AASHTO Road Test, to establish a thickness design (Minnesota Department of Transportation, 2012).

Some concrete pavement design methodologies use an erosion analysis in their calculation algorithms. The erosion analysis evaluates the potential for a concrete pavement to fail by pumping, erosion of the foundation support, and/or joint faulting, and is based on corner deflections. The primary failure observed at the AASHTO Road Test in the concrete pavements was pumping or erosion of the support layers. The Portland Cement Association (PCA) created the erosion model to limit the likelihood of this type of failure. The model is based on AASHTO Road Test results with additional faulting studies from several states, including Minnesota. The model evaluates the power or work done by the pavement system as a function of corner deflection, pressure at the slab-foundation interface, concrete modulus of elasticity and Poisson's ratio, slab thickness, and modulus of subgrade reaction (Minnesota Department of Transportation, 2012).

The service life of rolled concrete pavement constructions is directly related to the fatigue that develops over time from the loads affecting the pavement structure. Due to the loads affecting the pavement structure, stresses and deformations are formed in the layers of the pavement structure, which are the main cause of fatigue of the pavement structure. The RCC layer is a very important component of the pavement structure, since this layer must be sufficiently resistant to stress, deformation and fatigue (Mohammed et al., 2018b). The amount of stresses, deformations

and fatigue at the bottom of the RCC depends on the mechanical properties of the RCC. The most important mechanical properties of concrete are compressive strength, bending strength and splitting strength (Vaitkus et al., 2020). The flexural strength of typical hardened concrete after 28 days is 4.5–5.2 MPa, the compressive strength is 27.5–40 MPa (Vaitkus et al., 2019). The mechanical characteristics of rolled concrete are influenced by the composition of the rolled concrete mixture.

Sengun et al. (2021), while examining the fatigue of the RCC pavement structure, singled out the bending strength as one of the most important and critical aspects influencing the projected thickness of the RCC layer. Shiraz & Okamoto (1987) was among the first researchers to study the fatigue of RCC.

Shiraz & Okamoto (1987) testing on the mechanical properties of RCC showed that the most optimal one was the RCC mixture, which contained 55% of coarse aggregate (5–20 mm) and 45% of fine aggregate (0–5 mm), respectively. The design compressive strength of the RCC mixture after 28 days was 21 MPa, and the actual compressive strength after 28 days was 28–35 MPa. It was also concluded that fly ash had no appreciable effect on the compressive strength of the RCC mixture.

Shiraz & Okamoto (1987) in fatigue studies used beams cut from the experimental section (15×15×76 cm). Fatigue tests were performed 7 months after installation of the experimental section. During the fatigue test, the beams supported at three points were subjected to a cyclic load. The loads were chosen to produce a stress to flexural strength ratio between 0.5 and 0.95. During the test, the loading frequency was 10 cycles per second. Fatigue tests were terminated when the beam cracked. Shiraz & Okamoto (1987), after fatigue studies, designed a curvilinear relationship between the stress coefficient and the required loading number. To this day, the aforementioned dependence is used in the methodology for calculating the thickness of the concrete layer developed by the Portland Cement Association (PCA).

In 2003, the Canadian Cement Association conducted a study on the mechanical properties of RCC, the purpose of which was to determine the mechanical properties of different RCC mixtures and compare them with the mechanical properties of traditional concrete in terms of fatigue. Fatigue was evaluated by 3-point bending tests; tests were performed until the specimen failed or when one million loading cycles were reached. The research results showed that the fatigue resistance of RCC mixtures after one million loading cycles was 60% of its static flexural strength, 50% of traditional concrete, i.e., studies found higher fatigue resistance of RCC than traditional concrete (Sengun et al., 2021).

In 2013, the American Concrete Pavement Association (ACPA) developed a fatigue model for the design of RCC pavements. The RCC fatigue model was developed based on the RCC fatigue study conducted by 141 researchers. The developed RCC fatigue model compared with the PCC fatigue model, which was used in automated calculation programs, showed significant differences, so using the usual PCC fatigue model in the design of RCC pavements was not recommended (Roden, 2013).

One of the most recent RCC fatigue studies was performed by Sengun et al. (2021). The researchers used three different RCC mixtures in the fatigue study. Only the amount of binder differed in the RCC mixes, i.e., 200 kg/m^3, 400 kg/m^3 and 600 kg/m^3 were used and 0/12 fraction aggregate was used everywhere. Sengun et al. (2021) also used 55% fine aggregate (0–5 mm) and 45% coarse aggregate (5–12 mm) in RCC mixes. Coarse filler of 5–12 mm was chosen in order to obtain a smoother RCC surface and to reduce the risk of segregation. In order to simulate field compaction conditions, the researchers used a new compaction procedure they developed in the study (Sengun, 2019). After the concrete pouring was completed, the mixtures were cured in the mould under a wet damp cloth, and when the concrete became sufficiently stiff, beam specimens (10×15×35 cm) were cut from the slab and covered with a damp cloth for curing until testing (Sengun et al., 2021).

Sengun et al. (2021) in RCC fatigue tests first determined the ultimate flexural strengths of manufactured RCC mixes. In order to determine the maximum fatigue stresses, the obtained flexural strength values from three-point bending tests were multiplied by the adopted stress factors (55%, 62.5%, 70%, 77.5%, and 85%). During the test, the minimum fatigue load was 20% of the maximum flexural strength.

After determining the load parameters, a three-point bending stress test was performed with load control. Cyclic loading was applied at a frequency of 10 Hz (10 cycles per second) during the tests, and the fatigue test was continued until the specimen failed or when two million load cycles were reached. Two million load cycles are generally accepted as a sufficient number of cycles to determine the fatigue strength of plain concrete.

Mahdi et al. (2020) conducted an experimental fatigue study of an RCC pavement structure in which two different RCC pavement structures were installed under field conditions. The pavement structure consisted of a 20.3 cm thick RCC layer installed on a 30.5 cm stabilized base layer or 21.6 cm thick cement-improved soils and a 25.4 cm thick reinforced soil bed (Mahdi et al., 2020). A polymer plate was incorporated in the RCC pavement structure. 16 deformation sensors and 3 temperature sensors were placed in the polymer plate at different depths.

Load-induced deformations were measured using an ATLaS30 double tire load at different load magnitudes under both static and dynamic load conditions. For static loading, ATLaS30 twin tires were manually placed on the slab and the load was hydraulically applied to the RCC pavement section at four different load levels (40 kN, 72 kN, 89 kN and 112 kN). For dynamic loading, ATLaS30 dual tire loads were applied in both directions at a speed of 6.5 km/h with different load values after several passes. The recorded data was used to produce pools under different load conditions. Mahdi et al. (2020) used a finite element model to analyse the performance of engineered pavement structures. A finite element model was used to determine the critical stresses of the RCC layer under dynamic loading (Mahdi et al., 2020). Constructing the finite element model of the constructed pavement structures, the RCC layer was treated as elastic, and its stiffness moduli were adopted to be calculated by back-calculation from the measured deflections of the pavement surface with a falling weight deflectometer (HWD) (Mahdi et al., 2020). During the study, the deformations read from the deformation sensors installed in the pavement structure were compared with the deformations determined using the finite element model. The comparison revealed minor differences. Mahdi et al. (2020) also determined the critical stresses of the installed pavement structures at the bottom of the RCC layer, loading the centre and edge of the slab. Also, using the fatigue model it was determined how many repeated loads the pavement construction would withstand (Mahdi et al., 2020).

Many scientists have carried out detailed studies of traditional concrete fatigue using different concrete mix compositions and materials. Systematized fatigue functions are presented in Table 1. Meanwhile, the fatigue of rolled concrete is not so well studied by the scientist. Research conducted by researchers on the fatigue of rolled concrete shows different results. Some studies show that rolled concrete has similar fatigue properties as traditional concrete, other studies show that rolled concrete has a higher resistance to fatigue formation.

Taking into account the analysis of fatigue functions, the main and most commonly used mechanical property of concrete in the analysis of fatigue cracking is flexural strength. Flexural strength – the maximum measured resistance of a concrete specimen to a bending load. Some concrete pavement design methodologies use two different failure models: cracking analysis and erosion analysis. Erosion analysis when pavement fails by pumping, erosion of the foundation, or joint faulting is also a very important aspect that must be taken into account in concrete pavement design. The main property in the erosion analysis is the deflection at the corner of the concrete slab.

Table 1. Systemized fatigue functions

Source	Fatigue function	Required mechanical property	Analysis
The Portland Cement Association (PCA) (Okamoto, 1999)	$\log N_f = 11.737 - 12.077SR$, for $SR \geq 0.55$ $N_f = \frac{4.2577^{3.268}}{SR - 0.4325}$, for $0.45 < SR < 0.55$ N_f = unlimited, for $SR \leq 0.45$	Flexural strength	Fatigue cracking
The Portland Cement Association (PCA) (Okamoto, 1999)	$\log N_f = 14.524 - 6.777(C_1P - 9)^{0.103}$	Slab corner deflection	Erosion (pavement fails by pumping, erosion of foundation, joint faulting)
American Concrete Pavement Association (ACPA) (Roden, 2013)	$\log N_f = 14.524 - 6.777(C_1P - 9)^{0.103} - \log C_2$	Slab corner deflection	Erosion (pavement fails by pumping, erosion of foundation, joint faulting)
American Concrete Pavement Association (ACPA) (Roden, 2013)	$\log N_f = \left[\frac{-SR^{-10.24}\log(1-P)}{0.0112}\right]^{0.217}$	Flexural strength	Fatigue cracking
Okamoto (1999)	$\log N_f = 17.61 - 17.61SR$	Flexural strength	Fatigue cracking
Parker et al. (1979)	$\log N_f = 2.13SR - 1.2$	Flexural strength	Fatigue cracking
Thompson et al. (1990)	$\log N_f = -1.7136SR + 4.284$, for $SR > 1.25$ $\log N_f = 2.8127 \times 1.2214SR$, for $SR < 1.25$	Flexural strength	Fatigue cracking
Modarres & Hosseini (2014)	$SR = 0.965 - 0.025\log(N)$, $R^2 = 0.94$	Flexural strength	Fatigue cracking
Graeff et al. (2012)	$SR = 1.268 - 0.1219\log(N)$, $R^2 = 0.77$	Flexural strength	Fatigue cracking
Sun et al. (1998)	$SR = 0.986 - 0.0693\log(N)$, $R^2 = 0.97$	Flexural strength	Fatigue cracking
Sengun et al. (2021)	$SR = 0.911 - 0.047\log(N)$, $R^2 = 0.80$	Flexural strength	Fatigue cracking

1. Experiment

The experiment was divided into two parts. The first part of the experiment was focused on the environmental impact on the RCC pavement structure with cement and special additives stabilized base. In light of that, the strain dependency of roller compacted concrete pavement on cement stabilized base depending on the dynamic load and the season of the year was analysed. The data used in this part of the experiment was obtained from temperature-humidity sensors and a strain gauge installed in the pavement structure at different elevation. Deformations at the bottom of the RCC layer were measured by imitating a 200 kN load with a falling weight deflectometer (FWD). Pavement structures with cement stabilized base and RCC on top usually have high bearing capacity, because of that 200 kN load was selected to achieve bigger and more noticeable variation at different seasons.

The second part of the experiment was focused on fatigue and erosion (faulting) analysis. The main aim of the second part of the experiment was to verify and compare load cycles to failure of the pavement structure calculated according to the theoretical data obtained at the design stage of the pavement structure and data obtained from the experimental section of local road No. 130. Fatigue, erosion (faulting) analysis was carried out according to formulas from the literature analysis (more information is provided in Table 1). Data used in this part of the experiment was obtained from the strain gauge installed at the bottom of the RCC layer and from bearing capacity tests carried at the corners of the concrete slab on the local road No. 130. In this part of the experiment, a 50 kN load was imitated with a falling weight deflectometer, which corresponds to the typical one-wheel load used in pavement design in Lithuania.

1.1. Test site

The experimental section of the RCC pavement with cement and special additives bounded base layer and subbase is installed on the Lithuanian local road No. 130 (4–2V). Local road No. 130 (4–2V) was reconstructed in June–August 2021. The length of the reconstructed local road No. 130 (4–2V) was 699 m, the width of the concrete pavement 10 m, the unbound shoulders – 1 m. The experimental section starts from the bridge over the river of Žeimena and ends slightly further the railway crossing (more information is provided in Figure 1).

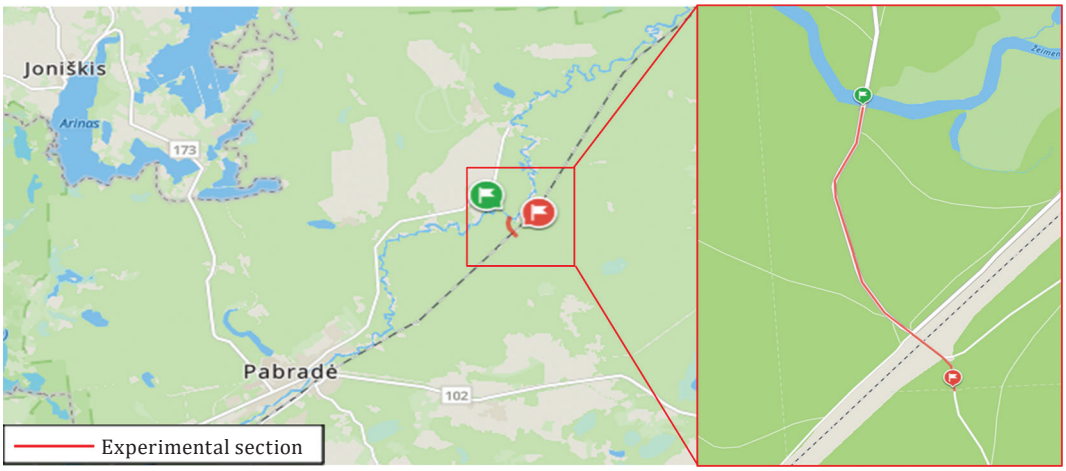

Figure 1. Test site location

1.2. Pavement structure design

The pavement structure design of the local road No 130 was performed according to the concrete pavement design methodology of the American Concrete Pavement Association (ACPA) implemented in the StreetPave concrete pavement design software. At the stage of the pavement design, cracking analysis model when the pavement fails due to the developed fatigue in the concrete slab, and erosion (faulting) analysis model when the pavement fails due to pumping, erosion of foundation or joint fault, were investigated. Cracking analysis was performed according to the American Concrete Pavement Association (ACPA) fatigue function (Roden, 2013) given in Table 1, where: N_f – allowable repetitions; SR – stress ratio; P – probability of failure.

Erosion (faulting) analysis was performed according to the American Concrete Pavement Association (ACPA) (Roden, 2013) fatigue function given in Table 1, where Nf – allowable repetitions; C_1 – adjustment factor which depends on base/subbase type (untreated or stabilized); P – power; C_2 – adjustment factor which depends on shoulder type (without concrete shoulder or with tied concrete shoulder).

Input data of the calculation software StreetPave is presented in Table 2.

Output data of the calculation software is presented in Table 3.

Table 2. Input data of the design software StreetPave

Parameter	Value
Terminal Serviceability[1)]	2
Reliability[2)]	85
CBR of subgrade	5%
Percent of slab cracked at the end of design life	15%
Thickness of cement and special additives stabilized subbase layer (CTS)	20 cm
Modulus of elasticity of cement and special additives stabilized subbase layer (CTS)	400 MPa
Thickness of cement and special additives stabilized base layer (CTB)	40 cm
Modulus of elasticity of cement and special additives stabilized base layer (CTB)	900 MPa
k value below concrete slab	209.8 MPa/m
Flexural strength of concrete	5.5 MPa
Design period	20 years
Total sum of equivalent standard (10 t weight) axle loads	1.15 mln. ESAs
Dowels	–

Note:
1) Terminal Serviceability – is the point at which the pavement needs rehabilitation of some sort, such as restoration, resurfacing, or reconstruction.
2) Reliability – factor of safety of the pavement design.

Table 3. Output data of the design software StreetPave

Parameter	Value
Expected repetitions[1)]	0.47 mln.
Stress ratio (*SR*)[2)]	0.45
Allowable repetitions according to the cracking analysis	298.3 mln.
Power (*P*)[3)]	59.36
Allowable repetitions according to the erosion (faulting) analysis	0.54 mln.
Min. required thickness of the undoweled concrete	15.5 cm
Design thickness of the undoweled concrete	16 cm

Note:
1) Expected repetitions of load which causes 2.45 ESAs during the design period of 20 year.
2) Stress ratio (*SR*) is equal applied stress/allowable stress.
3) Power (*P*) is a function of corner deflection, pressure at the slab-foundation interface, concrete modulus of elasticity and Poisson's ratio, slab thickness, and modulus of subgrade reaction.

1.3. Pavement structure

At the stage of pavement construction, existing pavement materials (gravel 0/11–0/32 fraction, proctor density 1.73 Mg/m^3) were used for subbase and base layers, which were stabilized with cement and special additives. The pavement structure of the local road No. 130 is presented in Figure 2 and consists of:

- 16 cm of RCC layer;
- 40 cm cement and special additives stabilized base layer;
- 20 cm cement and special additives stabilized subbase layer;
- subgrade.

RCC mixture was produced in mobile concrete batching plant and consists of:

- 4/16 fraction crushed aggregates (48.8%);
- 0/4 fraction fine aggregates (30.9%);
- cement (14.7%);
- water (5.5%);
- concrete plasticizer (0.07%).

Cement and special additives stabilized base consists of:

- 3–8% portland cement;
- ion exchange enhancing chemical additive (0.2 l per m^3 of soil);
- water;
- soil.

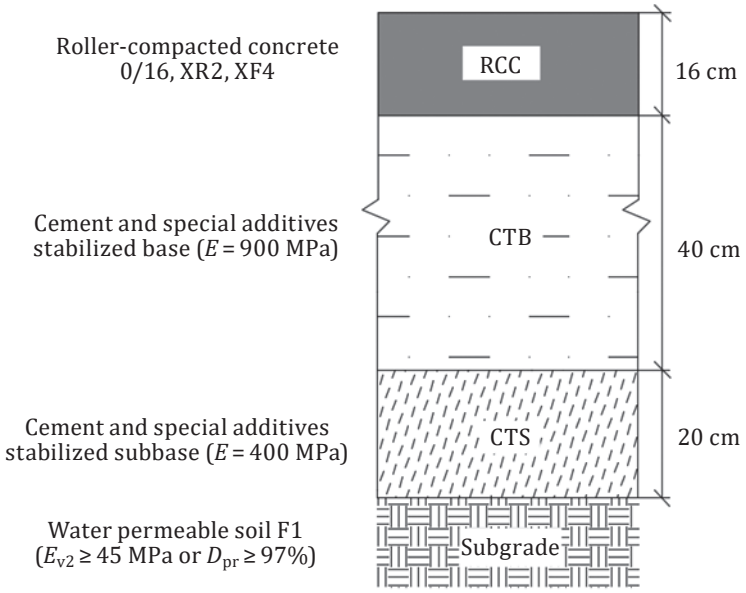

Figure 2. Pavement structure

Requirements for cement and special additives stabilized subbase:

- compressive strength after 28 days not less than 1.5 MPa;
- the ratio of compressive strength of samples after refrigeration and thawing cycles to reference samples (after 28 days) is at least 0.6;
- compaction rate not less than 98%.

Cement and special additives stabilized subbase consists of:

- 3–5 % portland cement;
- ion exchange enhancing chemical additive (0.2 l per m^3 of soil);
- water;
- soil.

Requirements for cement and special additives stabilized subbase:

- deformation modulus $Ev_2 \geq 100$ MPa;
- compressive strength after 28 days not less than 1.0 MPa;
- compaction rate not less than 98%.

Main characteristics of ion exchange enhancing chemical additive:

- the value of hydrogen ion concentration in pH – 1;
- pH (49 g/l, 25 °C) – < 1;
- fume pressure mm HG – 0.001;
- density, kg/l – 1.835;
- freezing/melting temperature – from –1.11 °C to –3.0 °C;
- viscosity (20 °C), mPas – 22.5.

1.4. Sensors

During reconstruction of the local road No. 130, in two different locations (250 and 350 m from the beginning of the reconstructed section) temperature-humidity sensors and a strain (deformation) gauge were installed in the pavement structure. Sensors were installed on the left side of the path of the road, in the right wheel (2.5 m from the road axis).

In location No. 1, the following sensors were installed:

- strain gauge (deformation sensor) and temperature-humidity sensor at the bottom of the RCC layer (16 cm deep from the surface);
- strain gauge (deformation sensor) and temperature-humidity sensor at the bottom of the cement and special additives stabilized base layer (at a depth of 56 cm from the surface).

In location No. 2, the following sensors were installed:

- strain gauge (deformation sensor) at the bottom of the RCC layer (16 cm deep from the surface);

– strain gauge (deformation sensor) and temperature-humidity sensor at the bottom of the cement and special additives stabilized base layer (at a depth of 56 cm from the surface).

Strain gauge (deformation H-shape) and temperature-humidity sensors were installed in the transverse direction with respect to vehicle traffic. Sensors at the bottom of the CTB and RCC layers were installed during reconstruction of the local road No. 130. Immediately after stabilization of the CTB layer (before compaction) at the planned sensors locations, the CTB layer was excavated in full depth, sensors were placed, about 5–7 cm of stabilized material was poured over the sensors and using a steel plate compacted with light human power. The rest of stabilized material was poured and compacted mechanically. During the installation of sensors under the RCC layer, trenches were prepared by cutting the CTB layer to the respect with sensors shapes and after that the RCC layer was laid with paver. The arrangement and installation of the sensors of the experimental section is shown in Figure 3.

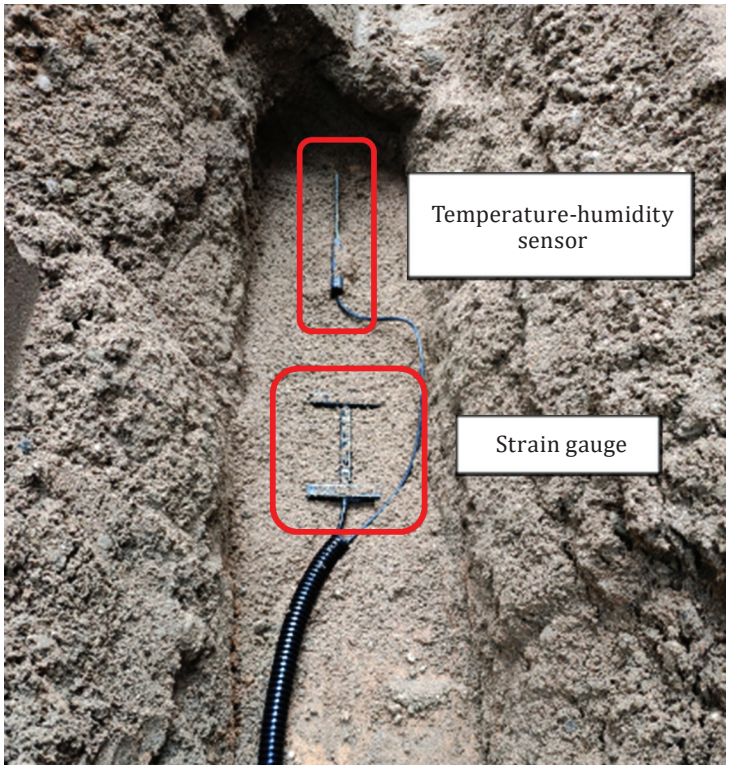

Figure 3. Location (installation) of sensors in the pavement structure

On the other side of the ditch, boxes are installed where the sensor cables are taken out and data loggers are installed. Temperature-humidity data is recorded continuously, i.e., every hour. Deformations at the bottom of the RCC layer and at the bottom of the cement and special additives stabilized base are recorded during the test, when the load is applied to the pavement structure.

The main specifications of the installed strain gauge are presented in Table 4.

The main specifications of the installed temperature-humidity sensor are presented in Table 5.

Table 4. Specifications of the strain gauge

Type	PAST II (For AC or PCC)
Range	Up to 1500 mstrain
Configuration	Single strain gage (1/4 brigde)
Cell material	Epoxy–Fiberglass
Coating	Epoxy–Silicone–PFT–Titanium
Resistance	120 Ω ±1.0 %; *GF* = 2.0
Voltage	Up to 12V (full bridge)
Temperature	–30° to 150 °C
∑E-modulus	≈ 2200 MPa
Cross section	$n \approx 0.5$ cm^2
Cell Force	0.110 N/mstrain
Fatigue life	Theoretically up to 108 cycles
Service life	Typically > 36 months

Table 5. Specifications of the temperature-humidity sensor

Measurement frequency	> 150 MHz
Measurement principle	TDT (time domain transmission)
Measurement signal	Symmetric, bipolar, differential
Measurement range	0–100% VWC (volumetric water content)
Accuracy soil moisture measurement	Typ. ± 2% in reference soil up to 50% VWC
Accuracy soil moisture measurement	Typ. ± 3% in reference soil up to 100% VWC
Accuracy temperature measurement	Typ. ± 0.5 °C full range

1.5. Temperature and humidity monitoring

The temperature and humidity data used in this study were monitoring for two years (2022 and 2023) at two different locations (location No. 1 and location No. 2) with small gabs due to some technical issues. Furthermore, the temperature-humidity sensor installed under the RCC layer has failed approximately after one year of exploitation, so no data is presented for temperature and humidity of the 2023 at the bottom of RCC layer in this study. The temperature and humidity were monitored each hour and every day. Due to the large data obtained, data analysis was performed calculating average temperature and humidity levels. The average weekly temperatures at the bottom of the cement and special additives stabilized base (CTB) and at the bottom of the roller-compacted concrete (RCC) at location No. 1 are presented in Figure 4. Average weekly humidity levels at the bottom of the cement and special additives stabilized base (CTB) and at the bottom of the roller-compacted concrete (RCC) at location No. 1 are presented in Figure 5.

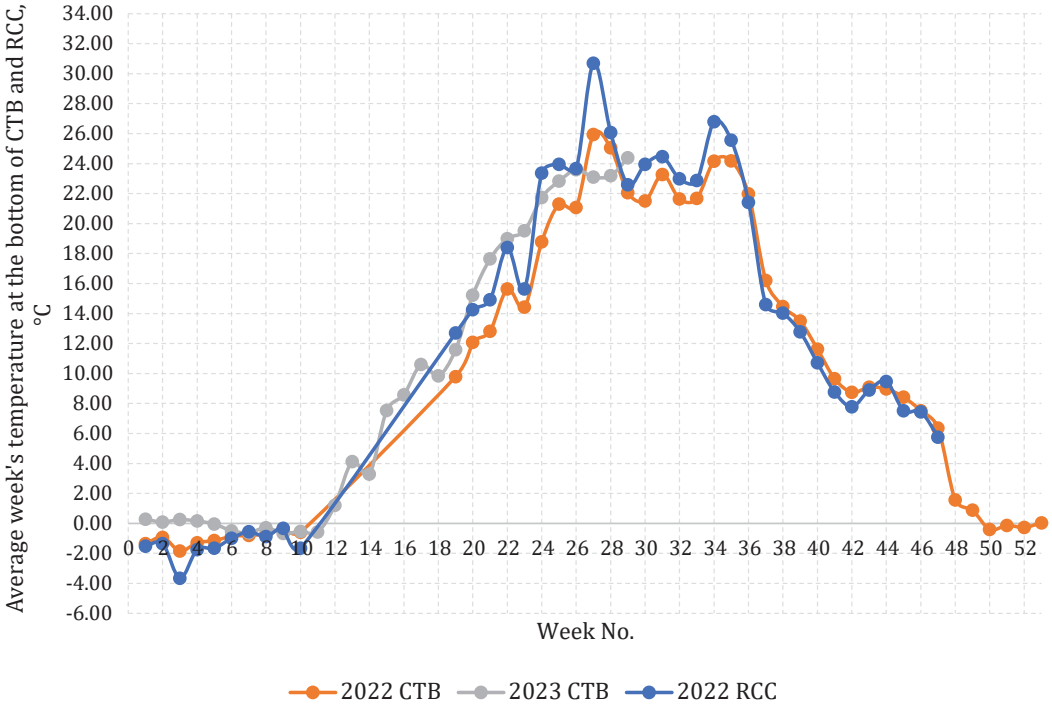

Figure 4. Average weekly temperatures at the bottom of the CTB and RCC at location No. 1

The average weekly temperatures at the bottom of the cement and special additives stabilized base (CTB) at location No. 2 are presented in Figure 6. Average weekly humidity levels at the bottom of the cement and special additives stabilized base (CTB) at location No. 2 are presented in Figure 7.

Statistical analysis of the monitored temperatures and humidity levels according to the different seasons of 2022 and 2023 are presented in Tables 6–9.

According to the Lithuanian Hydrological Service, the first 10 weeks of 2023 had air temperature above 0 °C and the first 10 weeks of 2022 had air temperature below 0 °C. Thawing started earlier in 2023 resulting in higher humidity in 2023 than in 2022 at the bottom of the cement and special additives stabilized base (CTB) at locations No. 1 and No 2.

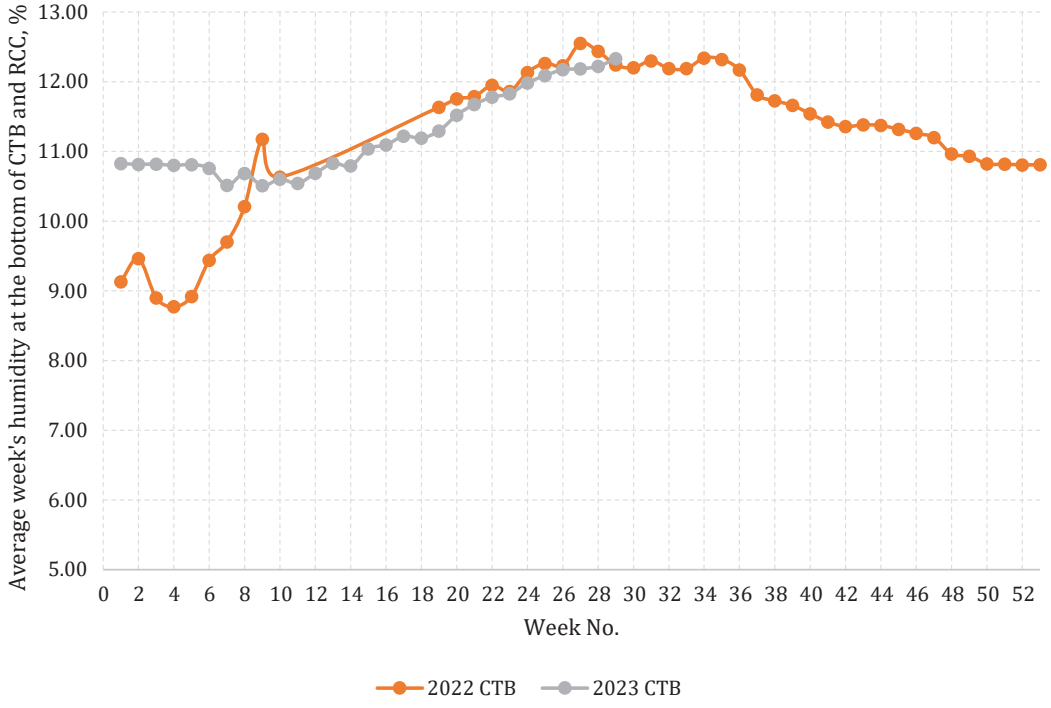

Figure 5. Average weekly humidity levels at the bottom of the CTB and RCC at location No. 1

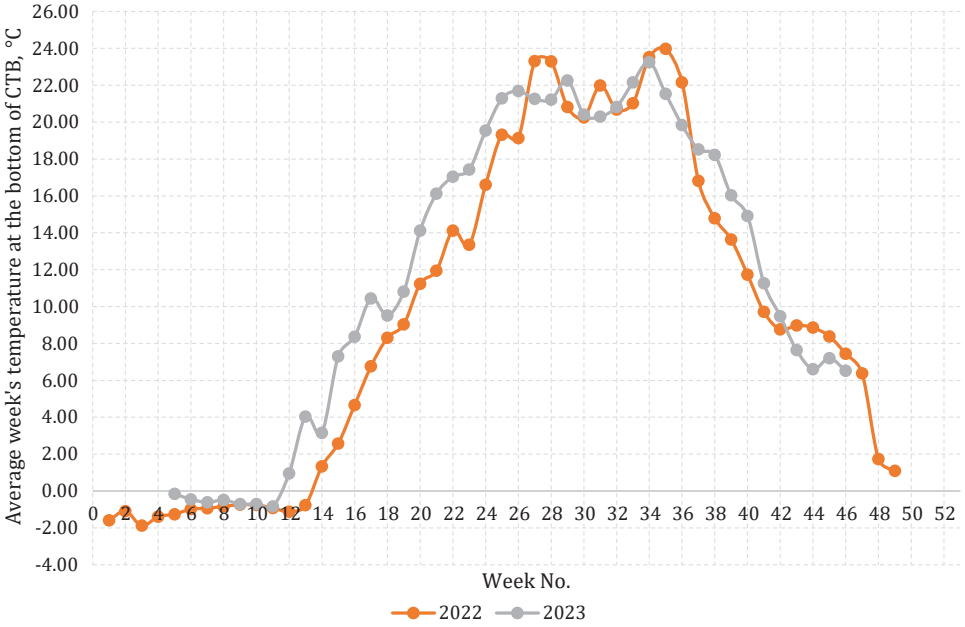

Figure 6. Average weekly temperatures at the bottom of the CTB at location No. 2

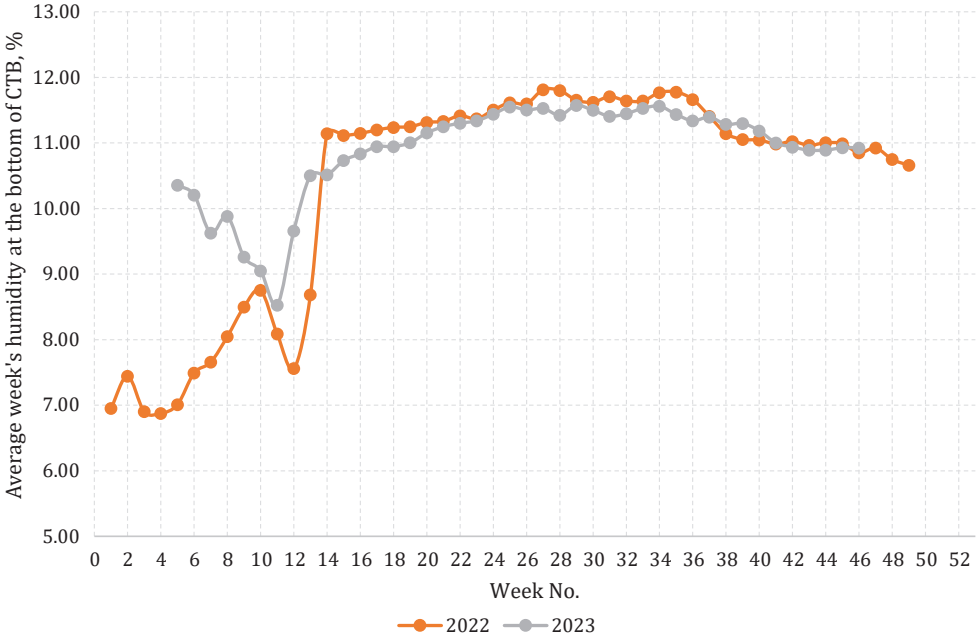

Figure 7. Average weekly humidity levels at the bottom of the CTB at location No. 2

Table 6. Statistical indicators of the monitored average seasonal temperatures at location No. 1

Season	2022								2023			
	Temperature at the bottom of CTB, °C				Temperature at the bottom of RCC, °C				Temperature at the bottom of CTB, °C			
	Min	Max	Average	SD	Min	Max	Average	SD	Min	Max	Average	SD
Spring	–0.80	16.93	11.02	5.44	–2.18	20.08	12.73	6.54	–0.77	19.46	7.52	6.30
Summer	14.17	27.67	22.25	2.72	15.71	31.74	24.36	3.21	17.37	25.98	22.39	1.82
Autumn	0.97	21.32	9.64	4.54	2.82	19.31	10.22	3.30	–	–	–	–
Winter	–2.94	1.00	–0.68	0.60	–7.34	–0.22	–1.39	1.23	–0.76	0.32	–0.11	0.36

Table 7. Statistical indicators of the monitored average seasonal humidity levels at location No. 1

Season	2022				2023			
	Humidity at the bottom of CTB, %				Humidity at the bottom of CTB, %			
	Min	Max	Average	SD	Min	Max	Average	SD
Spring	10.00	12.04	11.59	0.56	10.30	11.80	11.04	0.39
Summer	11.84	12.64	12.26	0.16	11.68	12.45	12.09	0.18
Autumn	10.93	12.12	11.42	0.27	–	–	–	–
Winter	8.38	11.26	10.03	0.88	10.34	10.83	10.75	0.11

Table 8. Statistical indicators of the monitored average seasonal temperatures at location No. 2

Season	2022				2023			
	Temperature at the bottom of CTB, °C				Temperature at the bottom of CTB, °C			
	Min	Max	Average	SD	Min	Max	Average	SD
Spring	–1.17	14.97	5.50	5.41	–0.89	17.34	7.04	5.88
Summer	13.20	25.32	20.93	2.79	15.86	24.45	20.90	1.71
Autumn	0.94	21.61	9.74	4.65	5.80	20.92	12.92	5.14
Winter	–2.99	1.22	–1.09	0.51	–0.67	–0.15	–0.50	0.14

Table 9. Statistical indicators of the monitored average seasonal humidity levels at location No. 2

Season	2022				2023			
	Humidity at the bottom of CTB, %				Humidity at the bottom of CTB, %			
	Min	Max	Average	SD	Min	Max	Average	SD
Spring	7.53	11.48	10.39	1.45	8.48	11.32	10.40	0.91
Summer	11.36	11.91	11.67	0.12	10.99	11.71	11.47	0.13
Autumn	10.03	11.65	11.01	0.28	10.61	11.47	11.12	0.22
Winter	6.39	10.81	7.59	0.76	9.56	10.37	9.91	0.29

1.6. Field testing

Deformation testing was conducted at the bottom of the roller-compacted concrete (RCC) by imitating a 200 kN load with a falling weight deflectometer (FWD) and obtaining deformation data from the installed strain gauge at the bottom of the roller-compacted concrete layer (RCC). Field testing was carried out at location No. 2 in November 2022 and November 2023. During the test pavement structure was loaded with 10 drops of 200 kN load and at each drop deformations were registered with a scan cycle of 0.001 s. The registered strains during each drop of 200 kN load are presented in Figure 8. In the time of deformation testing in November 2022 temperature at the bottom

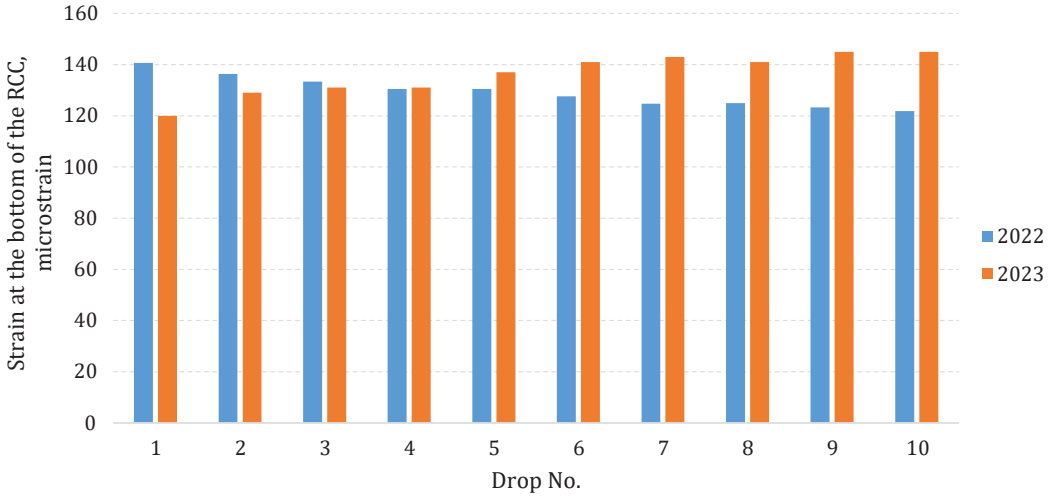

Figure 8. Strains at the bottom of RCC at location No. 2

of the cement and special additives stabilized base (CTB) was 7.90 °C, humidity – 11.14 %, in November 2023 temperature at the bottom of the cement and special additives stabilized base (CTB) was 6.31 °C, humidity – 10.95 %.

Statistical indicators of the deformation testing are presented in Table 10. In November 2022 at location No. 2 deformations at the bottom of the roller-compacted concrete (RCC) from 200 kN load imitated with falling weight deflectometer (FWD) varied from 122 microstrain to 141 microstrain, average was 129 microstrain and standard deviation – 6 microstrain. In November 2023 at location No. 2 deformations at the bottom of the roller-compacted concrete (RCC) from 200 kN load imitated with falling weigh deflectometer (FWD) varied from 120 microstrain to 145 microstrain, average was 136 microstrain and standard deviation – 8 microstrain.

Table 10. Statistical indicators of the deformation testing at location No. 2

Year	Min	Max	Average	SN
2022	122	141	129	6
2023	120	145	136	8

1.7. Stress at the bottom of RCC

According to the analysis of the literature, one of the main components of fatigue cracking formulas is the stress ratio (*SR*), which can be determined by dividing stress at the bottom of the concrete layer by the flexural strength of the concrete. Pavement structures that are designed to carry traffic loads are usually calculated taking into account the equivalent standard axle load, which is 10 t in Lithuania. Regarding the equivalent standard axle load, the strain at the bottom of the RCC was measured by imitating a 50 kN load with a falling weight deflectometer (load of one wheel). The deformation data was obtained from the strain gauge installed at the bottom of the RCC layer. The registered deformation at the bottom of the RCC layer from the 50 kN load imitated with a falling weight deflectometer (FWD) was 37 microstrain.

The stress at the bottom of RCC layer is equal to the 1.37 MPa and it was calculated according to formula (1):

$$\sigma = E \cdot \varepsilon, \tag{1}$$

where: σ – stress; E – elastic modulus of concrete (ERES, 1987); ε – strain.

1.8. Corner deflection

According to the analysis of the literature, one of the main components of erosion (faulting) formulas is corner deflection of the concrete slab. Data about corner deflections of the concrete slab was obtained by imitating a 50 kN load with a falling weight deflectometer (load of one wheel) at the corners of the slabs on local road No. 130. The corner deflection test showed that the average corner deflection on local road No. 130 was 167 μm. In the erosion (faulting) analysis carried out in this paper, average corner deflection plus one standard deviation was used, which is equal to 230 μm.

1.9. Calculations of load cycles to failure

The calculations of the load cycles to failure were made according to the fatigue functions presented in Table 1. Taking into account variables (*SR* and *P*) in fatigue functions, calculations were performed using data obtained from local road No. 130 and from theoretical calculations that were done at the design stage with design software StreetPave (more information is provided in Table 3). The stress ratio (*SR*) was calculated by dividing the stress determined at the bottom of RCC in local road No. 130 by the allowable stress (flexural strength of the concrete). Power (*P*) was calculated according to the corner deflection determined on local road No. 130, pressure at the slab-foundation interface, concrete modulus of elasticity and Poisson's ratio, slab thickness, and modulus of subgrade reaction function given in Table 1. The input data used in calculations of load cycles to failure is presented in Table 11.

The results of the load cycles to failure calculations are presented in Table 12.

2. Results and discussion

The comparison results of the average temperatures and humidity levels recorded in different seasons at location No. 1 are presented in Table 13. The comparison showed that the average temperature at the bottom of the cement and special additives stabilized base (CTB) in spring 2022 was 1.47 times higher than in spring 2023, in summer 2022 – 0.99 times lower, in winter – 6.42 times lower. The average humidity recorded at the bottom of the cement and special additives stabilized base (CTB) in spring 2022 was 1.05 times higher than in 2023, in summer – 1.01 times lower, in winter – 0.93 times lower.

Table 11. Input data in calculations of load cycles to failure

Variable	Theoretical (from StreetPave)	Local road No. 130 (from strain gauge or bearing capacity test)
Stress ratio, *SR*	0.45	0.25
Power, *P*	59.36	16.42

Table 12. Results of load cycles to failure calculations

Fatigue function	Required mechanical property	Analysis	Load cycles to failure, mln	
			Theoretical (from StreetPave)	Local road No. 130 (from strain gauge or bearing capacity test)
$\log N_f = 11.737 - 12.077\,SR$, for $SR \geq 0.55$ $N_f = \frac{4.2577^{3.268}}{SR - 0.4325}$, for $0.45 < SR < 0.55$ N_f = unlimited, for $SR \leq 0.45$	Flexural strength	Fatigue cracking	Unlimited	Unlimited
$\log N_f = 14.524 - 6.777\,(C_1 P - 9)^{0.103}$	Slab corner deflection	Erosion (faulting)	0.03	2.54
$\log N_f = 14.524 - 6.777\,(C_1 P - 9)^{0.103} - \log C_2$	Slab corner deflection	Erosion (faulting)	0.54	42.35
$\log N_f = \left[\frac{-SR^{-10.24}\log(1-P)}{0.0112}\right]^{0.217}$	Flexural strength	Fatigue cracking	298.3	Unlimited
$\log N_f = 17.61 - 17.61\,SR$	Flexural strength	Fatigue cracking	4847.30	Unlimited
$\log N_f = 2.13\,SR - 1.2$	Flexural strength	Fatigue cracking	0.00	0.00
$\log N_f = -1.7136\,SR + 4.284$, for $SR > 1.25$ $\log N_f = 2.8127 \times 1.2214^{SR}$, for $SR < 1.25$	Flexural strength	Fatigue cracking	0.00	0.00
$SR = 0.965 - 0.025\log(N)$, $R^2 = 0.94$	Flexural strength	Fatigue cracking	Unlimited	Unlimited
$SR = 1.268 - 0.1219\log(N)$, $R^2 = 0.77$	Flexural strength	Fatigue cracking	5.13	223.87
$SR = 0.986 - 0.0693\log(N)$, $R^2 = 0.97$	Flexural strength	Fatigue cracking	53.70	41686.94
$SR = 0.911 - 0.047\log(N)$, $R^2 = 0.80$	Flexural strength	Fatigue cracking	6309.57	Unlimited

The comparison results of the average temperatures and humidity levels recorded in different seasons at location No. 2 are presented in Table 14. The comparison showed that the average temperature at the bottom of the cement and special additives stabilized base (CTB) in spring 2022 was 0.78 times lower than in spring 2023, in summer 2022 and 2023 average temperatures were equal, in autumn 2022 – 0.75 times lower than in Autumn 2023, in winter 2022 – 2.17 times lower than in winter 2023. The average humidity levels recorded at the bottom of the cement and special additives stabilized base (CTB) in spring 2022 and 2023 were the same, in summer 2022 the average humidity was 1.02 times higher than in summer 2023, in autumn – 0.99 times lower, in winter – 0.77 times lower.

Comparison of the average temperatures recorded at different locations (Location No. 1 and No. 2) is presented in Table 15. The comparison showed that average temperature at the bottom of the cement and special additives stabilized base (CTB) at location No. 1 in spring 2022 was 2 times higher than at location No. 2, in summer 2022 average temperature was 1.06 times higher at location No. 1, in Autumn 2022 – 0.99 times lower than at location No. 2, in winter

Table 13. Comparison of the average temperatures and humidity levels in different seasons at location No.1

Season	Location No. 1	
	Temperature at the bottom of CTB (2022/2023)	Humidity at the bottom of CTB (2022/2023)
Spring	1.47	1.05
Summer	0.99	1.01
Autumn	–	–
Winter	6.42	0.93

Table 14. Comparison of the average temperatures and humidity levels in different seasons at location No. 2

Season	Location No. 2	
	Temperature at the bottom of CTB (2022/2023)	Humidity at the bottom of CTB (2022/2023)
Spring	0.78	1.00
Summer	1.00	1.02
Autumn	0.75	0.99
Winter	2.17	0.77

2022 – 0.62 times lower than at location No. 2. The average temperature at the bottom of the cement and special additives stabilized base (CTB) at location No. 1 in spring and summer 2023 was 1.07 times higher than at location No. 2, in winter 2022 – 0.21 times lower than at location No. 2.

Analysis of humidity levels recorded at the bottom of the cement and special additives stabilized base (CTB) at location No. 1 and location No. 2 showed that the RCC pavement structure with cement and special additives stabilized base had stable humidity around 12 % throughout the year with exception of the winter season when the humidity dropped to around 9.5%. The percentage of the humidity at the bottom of CTB can be affected by the early/late thawing period.

Comparison of the average humidity levels recorded at different locations (Location No. 1 and No. 2) is presented in Table 15. The comparison showed that the average humidity at the bottom of the cement and special additives stabilized base (CTB) at location No. 1 in spring 2022 was 1.12 times higher than at location No. 2, in summer 2022 average humidity was 1.05 times higher at location No. 1, in Autumn 2022 – 1.04 times higher at location No. 1, in winter 2022 – 1.32 times higher at location No. 1. The average humidity at the bottom of the cement and special additives stabilized base (CTB) at location No. 1 in spring 2023 was 1.06 times higher than at location No. 2, in summer 2023 the average humidity was 1.05 times higher at location No. 1, in Winter 2023 – 1.09 times higher at location No. 1.

According to the statistical indicators of deformation testing given in Table 10, the comparison of the deformations at the bottom of the roller-compacted concrete (RCC) of two different periods showed slightly higher (5.4 %) deformations in 2023 than in 2022. Slight changes in humidity at the bottom of the cement and special additives stabilized base had not any significant influence on the deformations at the bottom

Table 15. Comparison of the average temperatures and humidity levels at locations No. 1 and No. 2

Parameter	2022				2023			
	Season				Season			
	Spring	Summer	Autumn	Winter	Spring	Summer	Autumn	Winter
Temperature at the bottom of CTB (No. 1/ No. 2)	2.00	1.06	0.99	0.62	1.07	1.07	–	0.21
Humidity at the bottom of CTB (No. 1/ No. 2)	1.12	1.05	1.04	1.32	1.06	1.05	–	1.09

of the roller-compacted RCC layer. The slight difference in deformation at the bottom of the roller-compacted concrete (RCC) between two different periods could be influenced by the actual load size, which differed approximately by 5% from the target load of 200 kN.

Calculations of load cycles to failure of local road No. 130 using data obtained from the strain gauge demonstrated a stress ratio (*SR*), which resulted in a higher number of allowable repetitions according to a fatigue cracking analysis. Erosion faulting analysis of local road No. 130 showed huge differences between theoretical calculations and calculations using data obtained from bearing capacity tests of local road No. 130. Concrete pavements, especially without dowels and unstabilized or weak base are vulnerable to the faulting at the joints due to the poor load transfer between slabs. A stabilized base with compressive strength of 1.5–2.5 MPa creates sufficient support for the concrete and at the same time reduces stresses under the concrete by lowering pavement deflection. Joints in RCC pavement, formed by cutting 1/3 thickness of RCC slab, usually provide not less than 80% load transfer efficiency through aggregate interlock. Sufficient concrete support (lower pavement deflections) and sufficient load transfer efficiency through aggregate interlocking at the joints reduce the probability of failure due to erosion/faulting. Erosion/faulting fatigue function presented in Table 1 is sensitive for concrete pavements without dowels. The main reason why there is such a difference between service life against fatigue and erosion is that in the erosion/faulting function the foundation formed with stabilized layers and the load transfer efficiency of joints of RCC pavement without dowels is underrated.

Conclusions

The study of the stress and strain dependency of roller compacted concrete pavement on cement stabilized base dependent on dynamic load and season of the year resulted in the following conclusions:

- Monitoring of the temperature at the bottom of the cement and special additives stabilized base (at a depth of 56 cm) in roller-compacted concrete pavement structure showed an average temperature of 9.8 °C through the year (2022–2023) with a peak of 25.98 °C during summer and –2.99 °C during winter;
- Monitoring of the temperature at the bottom of the roller-compacted concrete RCC (at a depth of 16 cm) in spring 2022

showed an average temperature of 12.73 °C with a peak of 20.08 °C, in summer an average temperature of 24.36 °C with a peak of 31.74 °C, in autumn an average temperature of 10.22 °C with a peak of 19.31°C and in winter an average temperature of –1.39 °C with a peak of –0.22 °C;

- Monitoring of the humidity at the bottom of the cement and special additives stabilized base (at a depth of 56 cm) in roller-compacted concrete pavement structure through the year (2022–2023) showed variation from 7.53% to 12.04% and an average of 10.86% in spring, variation from 10.99% to 12.64% and an average of 11.87% in summer, variation from 10.03% to 12.12% and an average of 11.18% in autumn, variation from 6.39% to 11.26% and an average of 9.57% in winter;
- The average deformation measured with a strain gauge at the bottom of the roller-compacted concrete RCC (at a depth of 16 cm) from the load of 200 kN simulated with the falling weight deflectometer was 129 microstrain in 2022 and 136 microstrain in 2023. Slight changes in humidity at the bottom of the cement and special additives stabilized base did not have any significant influence on the deformations at the bottom of the roller-compacted RCC layer;
- Stress at the bottom of RCC layer determined from strain gauge by simulated 50 kN load with falling weight deflectometer (load of one wheel) was equal to 1.37 MPa and it was 1.80 times lower than theoretically calculated stress at the design stage with design software StreetPave;
- Calculations of load cycles to failure showed that for RCC pavement structures with cement and special additives stabilized base layer erosion (faulting) analysis was more critical than a fatigue cracking analysis;
- It is very important to study deformations at the bottom of the roller-compacted RCC layer with different flexural strengths of the RCC layer, which is the main property in pavement design. Imitation of traffic load with falling weight deflectometer and calculation of stresses at the bottom of the RCC layer using obtained deformations from the strain gauge can help learn more about performance of that kind of pavement structure and create a module of determination stresses at the bottom of the RCC using non-destructive testing.

REFERENCES

Chhorn, C., Hong, S. J., & Lee, S. W. (2017). A study on performance of roller-compacted concrete for pavement. *Construction and Building Materials*, *153*, 535–543. https://doi.org/10.1016/j.conbuildmat.2017.07.135

DieForschungsgesellschaft für Straßen- und Verkehrswesen. (2009). *Richtlinien für die Rechnerische Dimensionierung von Betondecken im Oberbau von Verkehrsf Lächen RDO Beton 09*. Die Forschungsgesellschaft für Straßen- und Verkehrswesen, Köln, German.

ERES. (1987). *Pavement design principles and practices*. National Highway Institute, Washington D.C., USA.

Fardin, H. E., & Goulart dos Santos, A. (2021). Predicted responses of fatigue cracking and rutting on roller compacted concrete base composite pavements. *Construction and Building Materials*, *272*, Article 121847. https://doi.org/10.1016/j.conbuildmat.2020.121847

Graeff, A., Pilakoutas, K., Neocleous, K., & Peres, M. (2012). Fatigue resistance and cracking mechanism of concrete pavements reinforced with recycled steel fibres recovered from post-consumer tyres. *Engineering Structures*, *45*, 385–395. https://doi.org/10.1016/j.engstruct.2012.06.030

Huang Yang. (2004). *Pavement analysis and design*. New Jersey, USA, Prentice-Hall, Pearson.

Lee, M. K., & Barr, B. I. G. (2004). An overview of the fatigue behaviour of plain and fibre reinforced concrete. *Cement and Concrete Composites*, *26*(4), 299–305. https://doi.org/10.1016/S0958-9465(02)00139-7

Lithuanian Hydrological Service. https://www.meteo.lt/

Mahdi, M., Liu, Y., Wu, Z., & Rupnow, T. (2020). Experimental investigation of wheel-load induced strain responses in roller compacted concrete pavements. In A. Chabot, P. Hornych, J. Harvey, & L. Loria-Salazar (Eds.), *Accelerated pavement testing to transport infrastructure innovation. Lecture notes in civil engineering*, *96*, Springer, Cham. https://doi.org/10.1007/978-3-030-55236-7_21

Minnesota Department of Transportation. (2012). *Use of street pave for design of concrete pavements for cities and counties in Minnesota*. Minnesota Department of Transportation, MN, USA. https://www.lrrb.org/pdf/201210.pdf

Modarres, A., & Hosseini, Z. (2014). Mechanical properties of roller compacted concrete containing rice husk ash with original and recycled asphalt pavement material. *Materials and Design*, *64*, 227–236. https://doi.org/10.1016/J.MATDES.2014.07.072

Mohammed, B. S., & Adamu, M. (2018a). Mechanical performance of roller compacted concrete pavement containing crumb rubber and nano silica. *Construction and Building Materials*, *159*, 234–251. https://doi.org/10.1016/j.conbuildmat.2017.10.098

Mohammed, B. S., & Adamu, M. (2018b). Evaluating the static and dynamic modulus of elasticity of roller compacted rubbercrete using response surface methodology. *International Journal of GEOMATE*, *14*(41), 186–192. https://doi.org/10.21660/2018.41.42833

National Concrete Pavement Technology Center. (2010). *Guide for roller-compacted concrete pavements*. Iowa, USA. https://rccpavementcouncil.org/wp-content/uploads/2016/08/CP-Tech-Center-RCC-2010.pdf

Okamoto, P. A. (1999). *Report on review of concrete fatigue models* (PCA R&D Serial No. 2213). Portland Cement Association, Skokie, Ill., USA.

Parker, F. Jr., Barker, W. R., Gunkel, R. C. & Odom, E. C. (1979). *Development of a structural design procedure for rigid airport pavements* (Report No. FAA-RD-77-8 1). Department of the Army and the Federal Aviation Administration, Washington, D.C., USA. https://www.tc.faa.gov/its/worldpac/techrpt/rd77-81.pdf

Papagiannakis, A., & Masad, E. A. (2008). *Pavement design and materials*. Hoboken, USA, John Wiley & Sons.

Rambabu, D., Sharma, S. K., & Akbar, M. A. (2023). A review on suitability of roller-compacted concrete for constructing high traffic resisting pavements. *Innovative Infrastructure Solutions*, *8*(1), 1–22. https://doi.org/10.1007/s41062-022-00989-4

Ramezanianpour, A. A., Mohammadi, A., Dehkordi, E. R., & Chenar, Q. B. (2017). Mechanical properties and durability of roller compacted concrete pavements in cold regions. *Construction and Building Materials*, *146*, 260–266. https://doi.org/10.1016/j.conbuildmat.2017.04.099

Roden, R. (2013). *RCC fatigue model development by the American Concrete Pavement Association (ACPA*) (Interim Report).

Sengun, E. (2019). *Effects of mixture design parameters and compaction methods on the properties of roller compacted concrete pavements* [PhD Thesis, Midle East Technical University]. https://etd.lib.metu.edu.tr/upload/12624703/index.pdf

Sengun, E., & Alam, B., Yaman, I., & Ceylan, H. (2021). A new evaluation of the fatigue design criteria of roller compacted concrete (RCC) pavements. *Construction and Building Materials*, *289*, Article 123195. https://doi.org/10.1016/j.conbuildmat.2021.123195

Sengun, E., Alam, B., Shabani, R., & Yaman, I. (2020). Strength and fracture properties of roller compacted concrete (RCC) prepared by an in-situ compaction procedure. *Construction and Building Materials*, *271*, Article 121563. https://doi.org/10.1016/j.conbuildmat.2020.121563

Shiraz, D. T., & Okamoto, P. A. (1987). Engineering properties of roller-compacted concrete. *Transportation Research Record*, *1136*, 33–45. https://onlinepubs.trb.org/Onlinepubs/trr/1987/1136/1136-004.pdf

Sun, W., Liu, J., Qin, H., Zhang, Y., Jin, Z., & Qian, M. (1998). Fatigue performance and equations of roller compacted concrete with fly ash. *Cem. Concr. Res*., *28*(2), 309–315. https://doi.org/10.1016/S0008-8846(97)00211-1

Thompson, M. R., Barenberg, E. J., Carpenter, S. H., Darter, M. I., Dempsey, B. J., & Ioannides, A. M. (1990). *Calibrated mechanistic structural analysis procedures for pavements*. Department of Civil Engineering, University of Illinois, Urbana-Champaign, USA.

Vaitkus, A., Kleiziene, R., Vorobjovas, V., & Čygas, D. (2019). Mixture strength class and slab dimensions' effect on the precast concrete pavement

structural performance. *The Baltic Journal of Road and Bridge Engineering*, *14*(3), 443–471. https://doi.org/10.7250/bjrbe.2019-14.452

Vaitkus, A., Škulteckė, J., Vorobjovas, V., & Šernas, O., & Žalimienė, L. (2020). Cement concrete modular pavement implementation for pedestrian and bicycle path. *IOP Conference Series: Materials Science and Engineering*, *987*, Article 012002. https://doi.org/10.1088/1757-899X/987/1/012002

Vaitkus, A., Gražulytė, J., Šernas, O., Karbočius, M., & Mickevič, R. (2021). Concrete modular pavement structures with optimized thickness based on characteristics of high performance concrete mixtures with fibers and silica fume. *Materials*, *14*(12), Article 3423. https://doi.org/10.3390/ma14123423